Multiscale entanglement clusters at the many-body localization phase transition

Loïc Herviou, Soumya Bera, and Jens H. Bardarson

Phys. Rev. B **99**, 134205 — Published 18 April 2019

DOI: 10.1103/PhysRevB.99.134205

Multiscale entanglement clusters at the many-body localization transition

Loïc Herviou,[1] Soumya Bera,[2] and Jens H. Bardarson[1]

[1] *Department of Physics, KTH Royal Institute of Technology, Stockholm, 106 91 Sweden*
[2] *Department of Physics, Indian Institute of Technology Bombay, Mumbai 400076, India*

We numerically study the formation of entanglement clusters across the many-body localization transition. We observe a crossover from strong many-body entanglement in the ergodic phase to weak local correlations in the localized phase, with continuous clusters throughout the phase diagram. Critical states close to the transition have a structure compatible with fractal or multiscale-entangled states, characterized by entanglement at multiple levels: small strongly entangled clusters are weakly entangled together to form larger clusters. The critical point therefore features subthermal entanglement and a power-law distributed cluster size. Upon entering the localized phase, the power-law distribution seems to persist with a varying power that crosses over into a stretched exponent before eventually becoming exponential deep in the localized phase. These results are in agreement with some of the recently proposed phenomenological renormalization-group schemes characterizing the many-body localized critical point, and serve to constrain other such schemes.

I. INTRODUCTION

Entanglement has been central in developing our current understanding of many-body localization (MBL)[1–4]. The many-body localization transition is fruitfully viewed as an eigenstate phase transition with eigenstates transitioning from area-law entanglement in the localized phase at strong disorder[5,6] to a volume-law entanglement in the ergodic phase at weak disorder[7,8]. The area law is a direct consequence of an emergent integrability in the localized phase[9–12] and eigenstates being product states of local integrals of motion[9,10,13–19]. This also results in the experimentally observed absence of thermalization[20–22], and slow growth of entanglement in quenches follows from dephasing induced by the exponentially decaying interactions between the integrals of motion[23–25]. The ergodic phase, in turn, exhibits slow dynamics[26,27], at least at small system sizes and short times, even in periodically driven systems[28,29], with a subballistic growth of entanglement. The subballistic entanglement growth is observed to slow down when approaching the transition and turns, at the critical point, into a logarithmic growth[23,24].

When it comes to the exact nature of the MBL phase transition the picture is less clear, and the transition has proven resilient to both numerical and analytical approaches. As a result, several phenomenological renormalization group (RG) approaches have been proposed[30–39], based on various physical assumptions on thermalization and random matrix theory. These approaches paint a different, albeit similar, picture of the critical point, where thermal and localized *clusters* of spins alternate or mingle. Here a cluster is to be understood as a subset of spins that is significantly less entangled with the rest of the system than within itself. The appearance of these clusters can be understood as a precursor of the emergent integrability and the local integrals of motions[9–15,18] characteristic of the MBL phase. Indeed, a completely disentangled cluster suggests the existence of conserved quantities, such as its total charge.

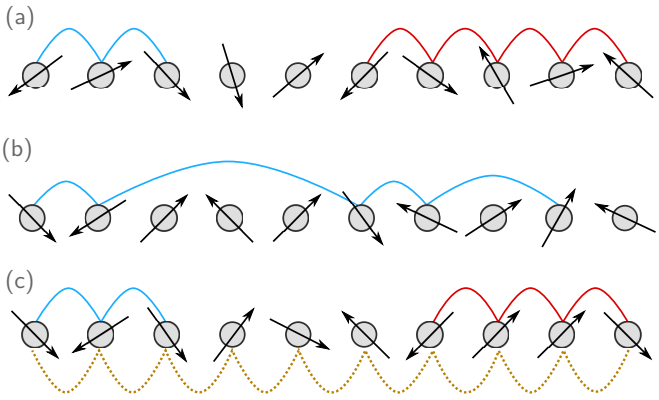

FIG. 1. Schematics for different types of entanglement structures obtained in different RG proposals. Black arrows represent spins, while the solid links mark entanglement between them. A set of spins connected by these links forms a single ergodic cluster, with different colors associated to different clusters. MBL clusters correspond to continuous sets of unconnected spins. The dotted lines mark a weaker entanglement. Though some residual entanglement survives in a MBL cluster, for simplicity, it is not represented here. (a) Ergodic and MBL connected clusters simply alternate. (b) One sparse ergodic cluster spans the entire chain. (c) Multiscale entanglement with small strongly entangled clusters (full lines) weakly entangled at a higher scale (dotted line) to form a larger cluster.

A distinguishing feature of the different RG proposals is their predicted structure of entanglement in eigenstates at the critical point. Three different proposals are depicted in Fig. 1: the first has alternating ergodic and localized clusters, each consisting of a consecutive sequence of spins[31]; the second suggests a dilute ergodic cluster that spans the entire chain, while most of the spins are localized[30,40]; the third multiscale (or fractal) state has a layered structure, with small ergodic and localized clusters joining up at a larger scale to form bigger clusters[32,35–37,39]. To determine which of these different scenarios best corresponds to the actual physics requires

identifying and analyzing the entanglement structure of eigenstates obtained from microscopic models. An algorithm for such identification is one of the main results of this work.

Thermal and many-body localized clusters can be identified by considering their entanglement properties. Indeed, in the ergodic phase, for a subsystem $\mathcal{A}$ of $n_\mathcal{A}$ spins, the (bipartite) von Neumann entanglement entropy

$$\mathcal{S}(\mathcal{A}) = -\mathrm{Tr}\ \rho_\mathcal{A} \ln \rho_\mathcal{A}, \tag{1}$$

where $\rho_\mathcal{A}$ is the reduced density matrix describing $\mathcal{A}$, takes a thermal value that depends on the energy density of the state and is linear in $l_\mathcal{A}$[41,42]. For middle of spectrum states, this thermal value is $n_\mathcal{A} \ln 2$ in the thermodynamic limit. The internal entanglement of the thermal clusters also follows this volume law, albeit with a possibly lower coefficient, due to finite-size effects. Many-body localized systems (and localized clusters) in contrast admit a lower entanglement entropy that follows an area law[5].

In this work, we study numerically the formation, properties and structure of clusters in a one-dimensional spin system, the XXZ spin chain in a random transverse field, commonly used to model many-body localization. Our method relies on an entanglement-based decomposition of the wave function and can be easily extended to more general models, including fermionic systems. Using a recursive search algorithm, we first identify the entanglement structure in the ergodic and localized phases. Entanglement in the ergodic phase is spread out over the entire system, without any local structure. In the localized phase, it is weaker and local: rare strongly entangled pairs appear even at strong disorder. The critical point can be identified by considering the characteristic sizes (number of spins and range) of the clusters. We show that the critical states admit multiscale entanglement that leads to a hierarchy of continuous clusters. This leads to subthermal entanglement and a power-law distributed cluster size at the critical point, in qualitative agreement with recently proposed RG schemes[34–37,39].

II. ENTANGLEMENT CLUSTER IDENTIFICATION AND CHARACTERIZATION

Ideally, to identify entanglement clusters, we should consider all possible partitions of the system and identify the one minimizing some appropriate multipartite entanglement measure. The factorial number of partitions and the general (at least) exponential cost of such entanglement measures make such an approach numerically infeasible, except for the very smallest of system sizes. Instead, we introduce an approximate recursive algorithm, restricting ourselves only to bipartite measurements, allowing us to achieve larger systems sizes while still capturing all the essential physics. To quantify the entanglement between two subparts $\mathcal{A}$ and $\mathcal{B}$ of an ensemble $\mathcal{A}\cup\mathcal{B}$, we use the normalized mutual information:

$$0 \leq i(\mathcal{A},\mathcal{B}) = \frac{\mathcal{S}(\mathcal{A}) + \mathcal{S}(\mathcal{B}) - \mathcal{S}(\mathcal{A}\cup\mathcal{B})}{\min(n_\mathcal{A}, n_\mathcal{B})} \leq 2\ln 2, \tag{2}$$

with $n_\mathcal{A}$ and $n_\mathcal{B}$ the number of spins in clusters $\mathcal{A}$ and $\mathcal{B}$ respectively. When $\mathcal{A}\cup\mathcal{B}$ is the total system, $i(\mathcal{A},\mathcal{B})$ reduces to twice the normalized entanglement entropy. Mutual information is a reliable tool to study the MBL phase transition as it distinguishes between wave functions with many-body entanglement, strongly-entangled pairs of spins, or localized spins[43–47].

As a first step towards identifying clusters, we represent the wave function as a binary tree with each node representing a set of spins. The root of the tree consist of all spins in the system. The first decomposition into two sets is identified by the bipartition of the system that minimizes the normalized mutual information. We then recursively search for the optimal decomposition of each set into two parts, until all sets are single-site, as illustrated in Fig. 2. We define the internal mutual information of a set as the normalized mutual information of its two descendants, i.e., the minimum amount of entanglement between all its bipartitions; for a single-site set, we take the internal mutual information to be its maximal possible value $2\ln 2$.

As the number of bipartitions of a system still scales exponentially, we further restrict the decompositions we evaluate: for each set we divide, we only consider bipartitions that would be continuous if the set was an isolated system, with all sites not contained in the set removed, and with periodic boundary conditions. To give a concrete example, if the current set consisted of sites $\{1,2,7,8,9\}$, the set $\{1,8,9\}$ would be a potential subset, while $\{1,7,9\}$ would not. This gives us the possibility to describe sparse sets at a low numerical cost, while retaining the ability to distinguish all the relevant structures observed in this paper. The normalization of the mutual information favors partitioning large localized sets before removing single spins from thermal sets or breaking strongly-entangled pairs.

The second step is to extract the cluster structure of the wave function from the binary tree. To do so, we introduce a mutual information cut-off i_cut, which one can think of as the minimum internal mutual information required for a set of sites to be considered an entangled cluster. This step is required to make quantitative our qualitative definition of a cluster as a set of spins that is significantly less entangled with the rest of the system than within itself. Alternatively it can be thought of as the control that determines when to stop subdividing clusters in the first step. Starting from the root, that is to say the whole system considered as a single cluster, we apply recursively the following rule: sets whose internal normalized mutual information is larger than this cut-off are kept as clusters, the rest are divided. The final stable ensemble of clusters is the cluster decomposition at the cut-off i_cut. Varying i_cut reveals the details of the entanglement structure of a state: at $i_\mathrm{cut} = 0$, the full

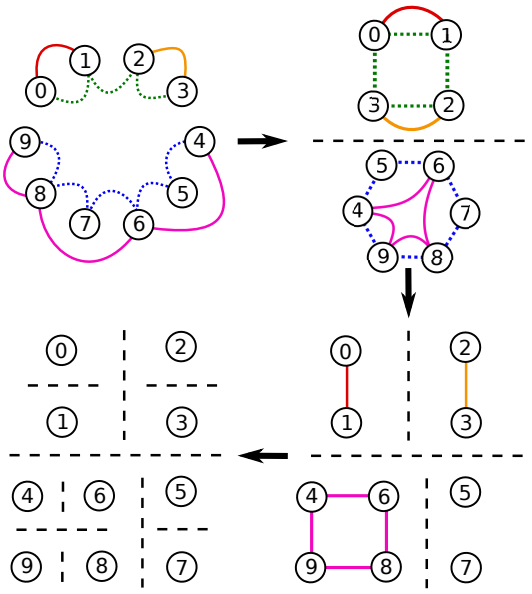

FIG. 2. Schematic description of the recursive algorithm used to identify entanglement clusters. The indexed circles represent physical sites, while links illustrate entanglement between sites. Dotted lines represent weaker correlations and the dashed lines the splitting into different clusters. The arrows mark one step of the algorithm, wherein the continuous bipartition that minimizes the mutual information is identified. We then apply the same process recursively to each so-obtained cluster.

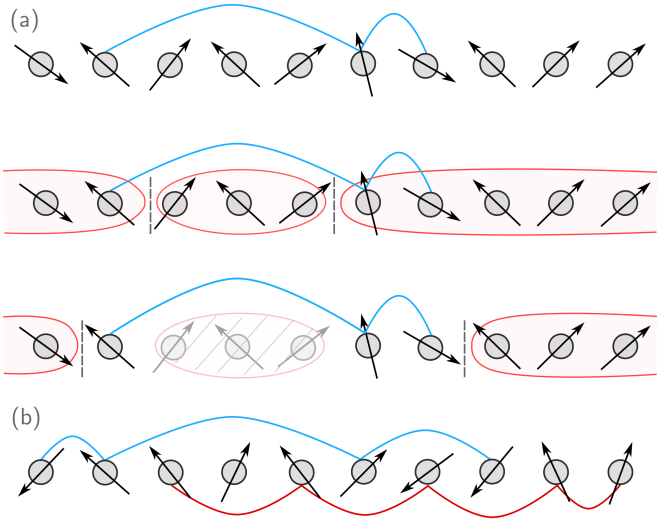

FIG. 3. a) We illustrate how the blue sparse cluster in the state depicted in the top row is extracted even when considering only bipartitions in continuous segments. In the first step, the system is partitioned into two sets, depicted in the second row, separating the three central spins $\{3,4,5\}$ from the rest of the system $\mathcal{A}=\{1,2,6,7,8,9,10\}$. When we further partition $\mathcal{A}$, the three central spins $\{3,4,5\}$ are no longer part of the current partition branch and are considered removed, and the set $\mathcal{A}$ is taken to be continuous and periodic. The bipartition of $\mathcal{A}$, depicted in the third row, now gives the blue cluster $\{2,6,7\}$, which is now considered continuous, and the rest $\{1,8,9,10\}$. b) An example of an entanglement configuration that is not captured by our approximate algorithm. The two intertwined clusters $\{1,2,6,8\}$ and $\{3,4,5,7,9,10\}$ cannot be separated as both of them are sparse over the same support.

system is considered to be a single cluster; with increasing i_{cut}, independent clusters progressively appear and are then broken down eventually into single-site sets, starting with the weakly entangled localized clusters.

A useful choice of i_{cut}, obtained by fixing the entanglement cut-off in each state to be equal to the internal mutual information i_{min} obtained at the first partition, results in what we call *minimal clustering*. The minimal clustering is not necessarily a simple bipartition of the total system: if one of the sets obtained after the first bipartition has smaller internal entanglement than the complete system, it will be further broken down. The minimal clustering gives additional information on how entanglement is spread throughout the system. In particular, it differentiates between many-body entanglement, with entanglement shared equally between all spins in a cluster, and resonant mechanisms where a spin couples with a single or few other spins.

Having obtained the clusters, we define the range l of a cluster $\mathcal{A}=\{x_1,...,x_n\}$ of n spins, with $x_1<x_2<...<x_n$, by

$$l = 1 + \min_{j=1,\dots,n} (x_j - x_{j+1} \mod L) \tag{3}$$

with $x_{n+1}=x_1$. While n is simply the number of sites in the cluster, l corresponds to the range of the system over which the cluster spreads. The spread controls the decay of correlation functions, as distant spins have nonzero long-range correlations if they are in the same cluster. The difference $l-n$ is a simple marker of the sparsity of a given cluster. Denoting with $[\,.\,]$ the average over clusters in a given state and $\langle\ .\ \rangle$ the average over states and disorder realizations, we define the average number of spins in a cluster $n_{\text{av}}=\langle[n]\rangle$, and the average maximum size of a cluster in a state $n_{\text{max}}=\langle\max\ n\rangle$. Analogous definitions hold for the range averages l_{av} and l_{max}.

The approximation to only consider continuous sets in the partition at each step is crucial for obtaining an efficient cluster decomposition, with a complexity $O(L^3)$ instead of $O(2^L)$. This exponential speedup is achieved without any significant loss in ability to correctly describe all relevant physical states. To back up this statement, we first verified that our algorithm distinguishes between all the entanglement structures described in Fig. 1, by applying it to randomly generated wave functions of each type and obtaining the expected outcomes, see App. A for data and more detailed discussion. The underlying reason for this is the recursive nature of the algorithm which allows to remove localized clusters interspersed within an ergodic cluster. For an example, consider the state in Fig. 3(a), which has one noncontinuous ergodic cluster with the remaining sites in insulating clus-

ters. The explicit steps in decomposing this state are as follows: in the first step the bipartition into the two sets $\{1, 2, 6, 7, 8, 9, 10\}$ (which is continuous because of allowed periodicity in the sets) and $\{2, 3, 4\}$ gives the minimal mutual information and thereby the first partition, denoted with red-colored ovals around the sites. The first of these sets is now considered a periodic and continuous set and has the bipartition into $\{1, 8, 9, 10\}$ and $\{2, 6, 7\}$, the second of which is the noncontinuous ergodic cluster. A continued application of the algorithm would, within the first step, further decompose these three clusters into smaller, eventually single site clusters. For the relevant value of the internal mutual information cut-off in the second step the ergodic cluster would, however, remain a cluster.

The only entanglement structure that we know our algorithm will fail to reproduce is one with intertwined thermal clusters, as depicted in Fig. 3(b). The algorithm would succeed in taking out the single site 4 but would then be left with the two distinct thermal clusters $\{1, 2, 6, 8\}$ and $\{3, 5, 7, 9, 10\}$ that can not be separated by any continuous bipartition. Such entanglement structure does, however, not seem very physical, and we would generally expect such clusters to merge into a single ergodic cluster in a physical system, which would be captured by our algorithm. This limitation of the algorithm therefore is not important. We verify that this is indeed true in small systems where we obtain identical results when relaxing the assumption of continuous clusters and computing the mutual information of all possible partitions; see Figs. A2, A3 and A4 in Appendix A. We therefore conclude that our algorithm accurately and efficiently captures the relevant physics.

III. CLUSTER STRUCTURE OF THE ERGODIC AND MBL PHASES

We apply our algorithm to the eigenstates of the XXZ spin chain in a transverse field, a common model of many-body localization[5,9,23,48–51], with Hamiltonian

$$H = -\sum_j \left(\sigma_j^+ \sigma_{j+1}^- + \sigma_j^- \sigma_{j+1}^+ + \frac{\Delta}{2} \sigma_j^z \sigma_{j+1}^z + h_j \sigma_j^z \right), \tag{4}$$

where σ are the Pauli matrices with $\sigma^\pm = (\sigma^x \pm i\sigma^y)/2$, Δ controls the interaction strength, and h_j is a random magnetization. We take periodic boundary conditions and denote with L the number of sites ranging from 10 to 16. Unless otherwise specified, we take $\Delta = 1$ and h_j^z uniformly distributed in $[-W, W]$. This Heisenberg limit admits a phase transition from an ergodic (metallic) phase to a many-body localized phase. The critical value of disorder in exact diagonalization studies of up to $L = 26$ spins is obtained as $W_c \approx 3.6$[48,51–54], while some matrix product state or Schmidt gap based approaches argue for a somewhat larger critical disorder strength[55–57]. We compute through exact diagonalization the 50 eigenstates with energies closest to the middle of the spectrum for 1000-5000 disorder realizations.

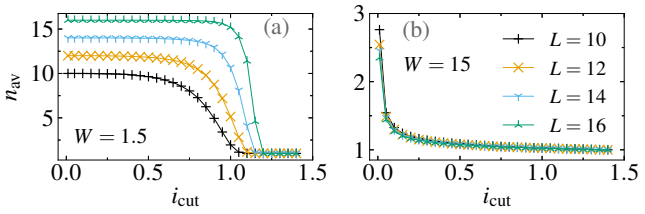

FIG. 4. Average number of sites n_{av} in a cluster as a function of mutual information cut-off for different system sizes for disorder strength $W = 1.5$ (a) and $W = 15$ (b). For $W = 1.5$, the system is ergodic and below the thermal value of i_{cut}, which is renormalized by finite-size, the complete system forms a single cluster; above this value, clusters become single-site. The abrupt transition marks true many-body entanglement and is a sign of ergodicity. For $W = 15$, the system is many-body localized. Even at low values of the entanglement cut-off, the system is fragmented into smaller clusters. With increasing mutual information cut-off, these clusters become smaller, with some resonating pairs surviving even at high cut-off.

Deep in the ergodic phase, the eigenstates have volume-law entanglement, shared equally between all sites. Consequently, after the first partition, the internal entanglement within each cluster will be smaller than i_{min}, and the minimal clustering corresponds to single-site clusters. Similarly, as long as i_{cut} is below the thermal value, our algorithm considers the chain as a single cluster. This behaviour is observed in Fig. 4(a). This transition from global to single-site clusters marks truly many-body entanglement and is characteristic of the ergodic phase in general.

In the MBL phase, the spins are very weakly entangled and $\langle i_{min} \rangle$ approaches zero as disorder increases. As we normalize the mutual information by the number of sites, minimal clusters have a length close to $L/2$. Some rare strongly entangled pairs are still present, with seemingly finite probability in the thermodynamic limit. Figure 5(a-b) shows the probability P_{pairs} for a cluster to consist of a pair of spins, and the probability $P_{pairs\ sep}(d)$ for the two spins in a pair to be separated by a distance d. We only observe short range pairs: for $W \geq 6$, around 90% of pairs correspond to neighbouring sites, while around 10% are separated by a single site. These ratios depend only weakly on i_{cut}, and we do not observe further separated pairs in any of our samples. The continuity of the measured clusters is presented in Fig. 5(c-d). In both phases, the difference between the range of a cluster and its number of sites is negligible. The probability $P_{discont}$ for a cluster to be discontinuous peaks close to the phase transition, but remains small (less than 5% for $i_{cut} = 0.35$). We essentially never observe a discrepancy between l and n larger than 2, at any cut-off.

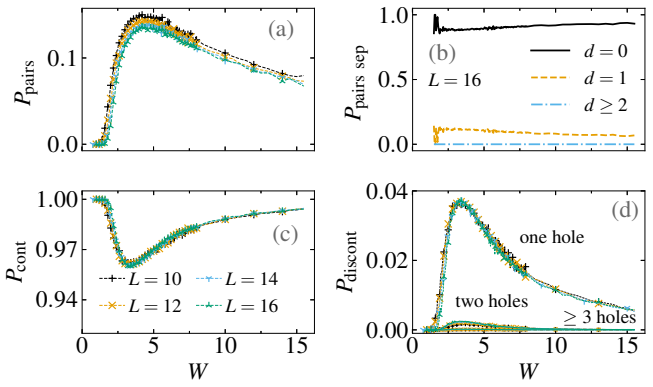

FIG. 5. (a) Fraction of clusters that consist of a pair of spins, and (b) fraction of pairs that are separated by d sites for $L = 16$, as a function of disorder strength. Resonant pairs are still present at high disorder strength (while the fraction of pairs decreases with system size, the number of clusters increases faster), but are short range with at most next-nearest neighbours. (c) Fraction of continuous clusters as a function of disorder strength. (d) Fraction of clusters with holes (here taken to be $l - n$); there are up to 4% with a single hole, less than 1% with two holes, and practically no clusters with a larger number of discontinuities. All data are obtained for $i_{\text{cut}} = 0.35$.

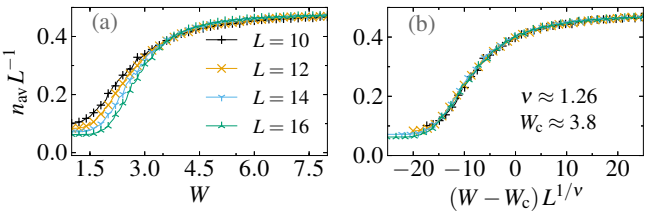

FIG. 6. (a) Mean length of minimal clusters as a function of disorder strength and (b) scaling collapse to the universal scaling form $n_{\text{av}} = L^{-1} f((W - W_c)L^{1/\nu})$. Similar results are obtained for the mean range. The collapse suggests that these quantities act as good order parameters for the MBL phase transition.

IV. CLUSTER STRUCTURE AT THE CRITICAL POINT

We plot in Fig. 6(a) the average length n_{av} of the minimal clusters, as a function of disorder strength. Both n_{av} and the average range l_{av} act as good scaling order parameters for pinpointing the ergodic to MBL phase transition, as they collapse remarkably well around the known critical point if rescaled by the total system length. The value of the critical disorder $W_c \approx 3.8$ is in good agreement with earlier studies, and the critical exponent is $\nu = 1.26 \pm 0.05$. As l_{av} and n_{av} scale linearly at the critical point, the Harris criterion under minimal assumptions[13,58] now translates into a bound $\nu \geq \frac{2}{d+2}$, consistent with the obtained exponent. Note that some recents studies[56,59] have found higher values of the exponent compatible with the standard Harris criterion. The quality of the scaling collapse is similar for different values of Δ, and the obtained exponents agree within the precision of our numerical analysis. This result therefore strongly suggests an extensive length of the minimal clusters at the phase transition.

At the phase transition, the minimal normalized mutual information i_{min} averages to 0.11 for $L = 16$, significantly lower than the thermal value, and decreases with system size. Our data is compatible with sublinear entanglement for this minimal bipartition: close to $W = 3.8$, $\langle i_{\text{min}} \rangle$ scales as $L^{-0.5 \pm 0.2}$, which is compatible with a power law scaling for the entropy of the minimizing cut $S(l_{\mathcal{A}}) \propto \sqrt{l_{\mathcal{A}}}$. Larger systems would be required to obtain a more precise bound on this exponent, since the minimal mutual information is subject to strong finite-size effects. Indeed, a finite-size-induced cross-over in the distribution of i_{min} is observed at much lower values of the disorder than the critical point, while a decent collapse for intermediate values of i_{min} is obtained in the critical region (see Appendix C 1 for more details). Recent computation[54] of the average entanglement in large-scale exact diagonalization nonetheless found it to be linear at the critical point. Though we cannot exclude that sparse thermal clusters do exist in the thermodynamic limit due to the small size of the considered system, the weak sparsity of the clusters at all disorder strengths, as shown in Fig. 5(c-d), strongly implies that this scenario does not occur. Though some clusters are disconnected, the difference between range and cluster length is essentially never larger than one, both in average and for the longest cluster of each chain, corresponding to a strong local impurity.

This picture of a weakly localized critical point is reinforced by an average and maximal cluster lengths that are both sublinear. We observe that the average mean length n_{av} diverges as $\ln L$ while the typical mean length $n_{\text{typ}} = \exp\langle[\ln n]\rangle$ is size-independent for $i_{\text{cut}} \geq 0.2$. This can be confirmed and understood by looking at the distribution of the cluster lengths, which follow a power-law until finite-size effects kick in, as shown in Fig. 7. The exponent increases with i_{cut}, but the power-law fitting is truly meaningful only for $0.15 \leq i_{\text{cut}} \leq 0.5$. Below this range, most systems are considered fully thermal, likely due to finite-size effects. Above it, clusters larger than a single site become rare events, and we would require a larger number of realizations to verify that the distribution is still a power-law. The exponent obtained in this meaningful regime is close to $\alpha = 2$. We further observe a large window of disorder strengths wherein the distribution is compatible with a power-law distribution, followed by a cross-over to a stretched exponential behaviour, as shown in Fig. 8. The power-law distribution survives even when studying the general fitting form $P(n) \propto n^{-\alpha} \exp(-\beta n^{\gamma})$: in a significant re-

gion around the critical point, we obtain $\gamma \approx 0$. At a fixed $i_{\rm cut}$, exponents depend only weakly on the disorder strength. While the finite-size effects at the tails of the distributions tend to diminish with increasing disorder strength, it remains unclear whether this indicates an actually higher value of the critical disorder, or if it is an effect of the cross-over.

At stronger disorder strength, the power-law becomes a stretched exponential decay before turning into a simple exponential at even higher disorder. The exponent of the stretched exponential varies continuously with disorder strength and, close to the critical point, takes a value close to the one obtained by Ref. 32 for correlation function decay in the localized fractal phase. Whether this cross-over is an actual phase transition between a finite-width critical region characterized by a power-law decay and a fractal localized phase characterized by a stretched exponential, or a simple finite-size crossover where only the critical region presents a power-law decay, cannot be directly assessed from our data. Larger system sizes tend to present a stretched exponential fit at weaker disorder strengths, but estimation of the width of the critical region at different sizes are too qualitative to be meaningful.

Finally, a qualitative comparison of the behaviour of the different characteristic lengths, both in a single state or averaged over disorder realizations, implies that critical states have a multiscale (or fractal) entanglement structure, as proposed in Refs. 32, 37, 39, 60–62. When increasing the entanglement cut-off for a given state, clusters progressively subdivide into smaller and smaller subclusters, instead of simply directly breaking down to single-site elements as in the ergodic phase. Some typical examples are presented in Appendix C 2.

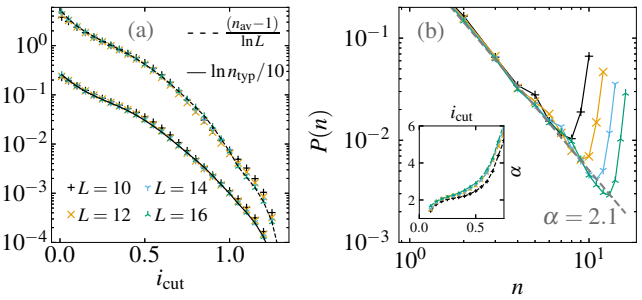

FIG. 7. Left panel shows the average length rescaled with logarithm of system size $(n_{\rm av}-1)/\ln L$ (top dotted line) and the logarithm of the typical length $\ln(n_{\rm typ})/10$ (bottom full line) at the critical point as a function of the cut-off $i_{\rm cut}$. The logarithm of the typical length has been rescaled for convenience, and the lines are guides to the eye. We observe a slowly divergent average length of a cluster, while the typical length is itself constant. Right panel shows the distribution of the cluster length for $i_{\rm cut} = 0.2$, with a decay as $l^{-\alpha}$, until finite-size effects kick in. The dotted line is the best power-law fit. All graphs are taken at the estimated critical point $W_c \approx 3.8$. In inset, we show the evolution of α when varying the cut-off for $L = 16$.

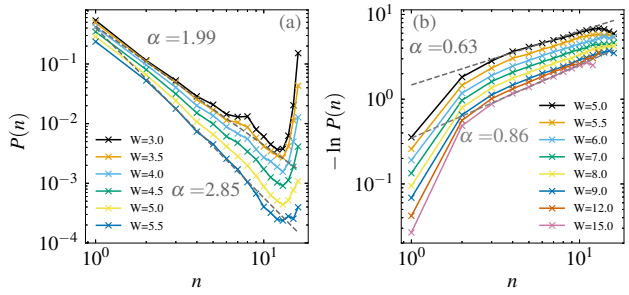

FIG. 8. Variation of the distribution of cluster lengths as a function of disorder strength, for $i_{\rm cut} = 0.2$ (similar results are obtained for $0.1 \leq i_{\rm cut} \leq 0.7$) and for $L = 16$. (a) Around the estimated critical point, we observe a large region compatible with a power-law probability distribution $P(n) \propto n^{-\alpha}$, with exponents that vary slowly with disorder strength. Note that a regression with $P(n) \propto \exp(-\beta\sqrt{n})$ also fits decently the intermediate cluster lengths. (b) At larger disorder strengths, the distribution becomes a stretched exponential $P(n) \propto \exp(-\beta n^{\alpha})$, with α going to 1 as disorder increases.

V. DISCUSSION AND CONCLUSIONS

We introduced a recursive numerical algorithm that allows the identification of entanglement clusters in wave functions. We used this algorithm to obtain and characterize the entanglement clusters in eigenstates of the XXZ Hamiltonian with a random field, which undergoes many-body localization at strong disorder. The cluster structure in the ergodic and MBL phases follow expectations: large many-body entanglement in the ergodic phase, which turns into a set of weakly entangled spins, with a few resonant pairs in the localized phase. As a general rule, clusters are formed by neighbouring sites, with occurrences of "holes" rare, even at the transition. Comparison with random states and analysis of the sparsity and structure of the clusters suggest a weakly localized critical point, with fractal or multiscale states. The distribution of cluster sizes at the critical point follows a power law with exponent close to 2. The power-law distribution of clusters seems to extend into the many-body localized phase, with a varying power eventually becoming a stretched exponential, and finally an exponential deep in the localized phase. Though the spin-chain is typically localized at the critical point, some rare extended regions survive, which leads to a logarithmic growth of the average cluster size.

Our work can serve to provide a microscopic justification and input into underlying assumptions of renormalization group type of descriptions of the many-body localization transition—it is therefore useful to compare with the current status of such calculations. Building on the simplified RG of Ref. 32, Goremykina et

al.[37] constructed an analytical RG scheme based on a strong asymmetry between localized and ergodic cluster in which ergodic clusters quickly absorb localized inclusions (motivated in part by the avalanche arguments of Refs. 35 and 36, which was later argued to lead to a similar physical picture[39]), while the properties of localized clusters are only weakly affected by incorporating small ergodic clusters. In this scheme the MBL transition is argued to be of a Kosterlitz-Thouless type, which leads to a power law distribution of ergodic cluster sizes at the critical point with an exponent that, interestingly, takes the value of 2 just as in our data. The cluster size distribution in the KT scaling picture remains a power law throughout the localized phase. On general grounds one expects the distribution to become exponential at large disorder strengths, prompting the question[39] of wether a second transition within the localized phase takes place or if the apparent power law close to the critical point is a stretched exponent that remains throughout the localized phase, smoothly turning into an exponential at strong disorder. While our data can not conclusively distinguish between the two scenarios, the power law fits are quite robust in a range of disorder values around the critical point, raising interesting questions about the nature of the localized phase. Naturally, we can not rule out that at very large system sizes that power laws turn out to be stretched exponentials.

In general, our results are qualitatively consistent with the results of recent RG proposals[34–37], which are mostly phenomenological approaches. The different scalings of the average and typical length of the thermal clusters was predicted by Ref. 37, while a non-universal power-law decay[34] followed by a stretched exponential behaviour was proposed by Refs. 35, 36, and 39. Conversely, Ref. 40 argued based on numerical arguments for the existence of a sparse thermal backbone. More precisely, by analyzing single-site entropies they inferred the existence of continuous sets of high-entropy sites, which formed local clusters, and then argued for (thermal) entanglement between these different clusters. Our numerical analysis indicates that these clusters should instead be considered independent. Nonetheless, both larger system sizes on the numerical side and a more microscopic approach on the renormalization side would be required for a careful validation. These new results should put strong constraints on similar renormalization schemes.

An exciting perspective, though numerically challenging, would be to extend this study to larger size system using matrix-product states[57,63–67] (from the localized side of the phase transition) or machine-learning based approaches[68]. The study of these clusters close to the phase transition may give a clearer answer on the nature of the phase transition, and the existence of a potential intermediate phase of a non-ergodic metal.[27,39,62,69–72] Extension of our results to higher dimensions, in particular to two-dimensions where tensor networks have been used to describe the MBL phase[73], is also relevant. A recent work on the mapping between excited localized eigenstates and ground states of disordered Hamiltonians[74] gives another promising means to numerically explore this problem. Properties of the entanglement clusters may shed light on the properties and stability of the many-body localized phase in this context.

ACKNOWLEDGMENTS

This work was supported by the ERC Starting Grant No. 679722 and the Knut and Alice Wallenberg Foundation 2013-0093. S.B. acknowledges support from DST, India, through Ramanujan Fellowship Grant No. SB/S2/RJN-128/2016. This research was supported in part by the National Science Foundation under Grant No. NSF PHY-1748958.

Appendix A: Verifying algorithm validity

The algorithm we introduced in the main text is based on a couple of approximations that at first sight may seem uncontrolled. In this appendix we demonstrate that it correctly identifies the structure of randomly generated wave functions, and that for small systems where we can calculate all bipartition the approximation of continuous clusters does not affect the results.

1. Randomly generated wave functions

We first show that our algorithm distinguishes between the entanglement structures described in Fig. 1, by applying it to randomly generated wave functions; the results are shown in Fig. A1.

The general process to create the random states is as follows: we first randomly select the sets of spins that are in independent thermal or localized clusters. Localized clusters are broken down to single-site clusters. Due to the $U(1)$ symmetry, we assign a fixed magnetization to each cluster, depending on its size, so that the complete system stays in the total $\sigma^z = 0$ sector. Then, for each cluster of size n and with magnetization m, we generate a uniformly distributed vector in the corresponding Hilbert space, which is the hypersphere of $\mathbb{C}^{\binom{n}{m+n/2}}$. The global wave function is then simply the (properly reordered) tensor product of these wave functions. Noise can be added by taking superpositions of such vectors, that can either be different realizations of the same cluster decomposition, or have entirely different structures. Though our results in Fig. A1 are presented without such noise, we verified they survive the added disorder.

In Fig. A1(a), we create continuous independent clusters, such that the probability for a cluster to be of length n decays as n^{-2}, to mimic the distribution observed at the critical point. The alternating ergodic and MBL structures are easily identified as the large ergodic clusters are still present at high values of i_{cut}, while the lo-

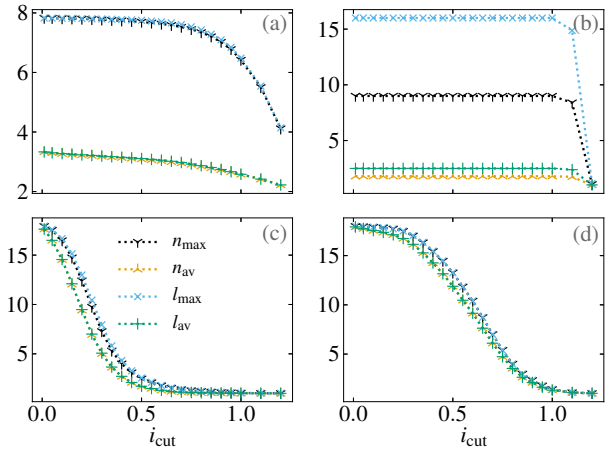

FIG. A1. The different characteristics lengths for random states of length $L = 18$, generated according the structures described in Fig. 1. In (a), ergodic clusters survive high entanglement cut-off, while the localized one are broken down quickly. In (b), the sparse ergodic cluster leads to a significant discrepancy between maximum range and maximum size. In (c-d), multiscale entanglement leads to a progressive separation of clusters into smaller ones, and the difference between average and maximum cluster length is much smaller. The difference between (c) and (d) lies in the probability distribution of wave function coefficients; see text for further details on how the random states are generated.

calized ones are reduced to a set of single-site clusters, resulting in a large difference between the average and maximum cluster sizes. We also performed a similar analysis by alternating thermal clusters taken as blocks of varying length n, separated by sets of localized spins treated as single-site clusters, without significant differences.

For Fig. A1(b), we randomly select a set of 9 spins that therefore spans most of the chain, and take the rest to be localized. The sparse ergodic cluster in this case leads to a significant difference between range and number of sites of the largest clusters. Varying the length of the sparse thermal cluster or introducing small thermal clusters does not affect the qualitative picture.

Finally, for Fig. A1(c-d), we create a multi-layered state in the following way. Let $\psi([s_1, s_2, ...], [m_1, m_2, ...])$ be the function that generates a random state associated to the cluster decomposition into sets s_j with magnetization m_j. Then, the states we study here are given by:

$$|\psi(m_1, ..., m_L)\rangle \propto \sum_{j=0}^{\lceil \ln_2 L \rceil} a_j \, |\psi_j\rangle \tag{A1}$$

with a_j uniformly distributed random variables taken between either 0 and $\frac{1}{j+1}$ [Fig. A1(c)] or between 0 and 1 [Fig. A1(d)], and

$$|\psi_j\rangle = \psi([[1 : 2^j], [1 + 2^j : 2^{j+1}], ...], [\sum_{k=1}^{2^j} m_k, ...]), \tag{A2}$$

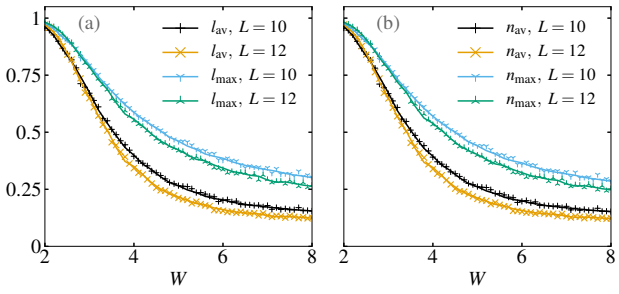

FIG. A2. Comparison of the different length scales—range in (a) and number of sites in (b)—between simulations where we evaluate the entropy on all bipartitions of the system (solid lines), and simulations where we only consider continuous partitions in each subset (symbols). We take $i_{\rm cut} = 0.2$. We observe a good agreement for all disorder strengths and all entanglement cut-offs we consider.

where $m_k = \pm\frac{1}{2}$ is the local magnetization. In other words, we create wave functions that are superpositions of random states organized as follows: $|\psi_1\rangle$ is a product state, while in $|\psi_{2\leq j<\lceil \ln_2 L\rceil}\rangle$ spins are entangled in consecutive sets of 2^{j-1} sites, each set being in a product state with the others. Finally, $|\psi_{\lceil \ln_2 L\rceil}\rangle$ is a random thermal state. Magnetization is chosen such that the $U(1)$ symmetry is respected at all scales, and that the different states are coherent with one another. Finally, we attribute a random weight to each $|\psi_j\rangle$. A simple minimal example for $L = 4$ is:

$$\begin{aligned}\left|\psi(\frac{1}{2},-\frac{1}{2},-\frac{1}{2},\frac{1}{2})\right\rangle \propto |\uparrow\downarrow\downarrow\uparrow\rangle + \frac{1}{2}(|\uparrow\downarrow\rangle - |\downarrow\uparrow\rangle)(|\uparrow\downarrow\rangle + |\downarrow\uparrow\rangle) \\ + \frac{1}{3}(|\uparrow\uparrow\downarrow\downarrow\rangle + |\downarrow\downarrow\uparrow\uparrow\rangle - |\downarrow\uparrow\downarrow\uparrow\rangle - |\uparrow\downarrow\uparrow\downarrow\rangle)\end{aligned} \tag{A3}$$

This hierarchy leads to a different dependence of n and l on $i_{\rm cut}$, with an initial fast decay followed by a slowing down when all weakly entangled clusters have broken down. In the localized phase, the decay is generally super-exponential with $i_{\rm cut}$, while multiscale wave functions can have exponential or stretched exponential behaviour, depending on the exact choice of the entanglement structure. When studying a single wave function, the clusters are progressively fragmented at very different cut-off strengths.

2. Including noncontinuous bipartitions

Our main algorithm assumes that intertwined thermal clusters are inexistent, or at best, rare and irrelevant events, as we limit ourselves to continuous subsystems in our recursive bipartitioning of the system. Two such intertwined clusters correspond to thermal clusters that

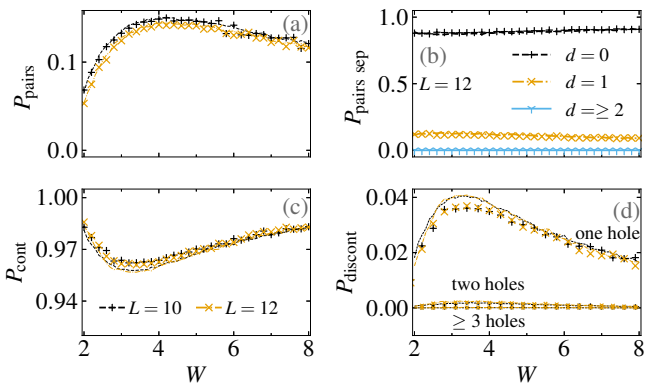

FIG. A3. In this figure, we compare the structure of the clusters obtained for small system sizes when checking all possible partitions (lines) to the one obtained using our main algorithm (markers). (a) Fraction of clusters that consist of a pair of spins, and (b) fraction of pairs that are separated by d sites for $L = 16$. (c) Fraction of continuous clusters as a function of disorder strength. (d) Fraction of clusters with holes (here taken to be $l - n$). Only the fraction of clusters with one hole is underestimated by less than 0.5%, while all other measures coincide. All data are obtained for $i_{\text{cut}} = 0.35$.

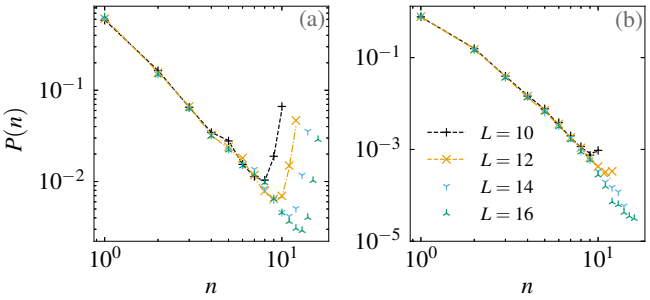

FIG. A4. In this figure, we compare the probability distribution of the clusters obtained for small system sizes when checking all possible partitions (lines) to the one obtained using our main algorithm (markers). Both panel shows the distribution of the cluster length for $i_{\text{cut}} = 0.2$. On the left, the distribution is taken for $W = 3.8$ and decays as a power-law until finite-size effects kick in. On the right, the distribution is taken for $W = 8$ and decays as a stretched exponential. For both disorder realizations, the two schemes agree.

mix (they have finite overlap inn their support) without thermalizing. Such a situation would be, at least for large inclusions, quite unphysical as thermal clusters would likely hybridize. We checked on small systems, where all bipartitions can be computed, the validity of this approximation. Figure A2 presents a comparison between the different length scales we obtain with our algorithm and the case when we compute the mutual information of all bipartitions. No significant differences are observed. Figure A3 presents the structure of the obtained clusters, and in particular, how sparse the clusters

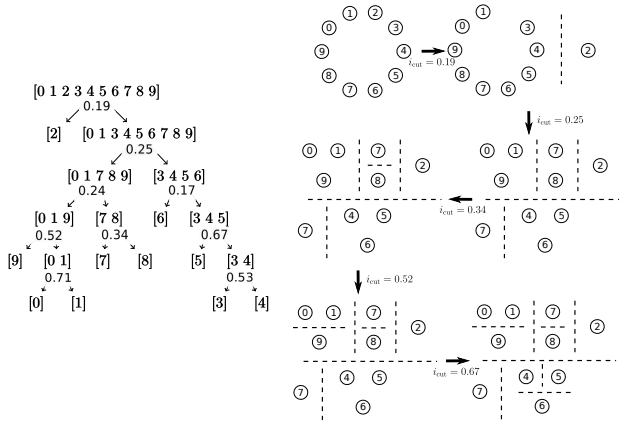

FIG. B1. Example of a decomposition into clusters by our algorithm (with $L = 10$ and $W = 3.7$). On the left, the binary tree we obtain, with each node corresponding to a set of spins labelled by the sites it includes (here from 0 to 9). Sets are divided into subsets following the edges of the tree. The label on the edges corresponds to the normalized mutual information between its two descendants. On the right, a schematic picture of the progressive appearance of clusters when varying the mutual information cut-off i_{cut}, applied to the binary tree on the left. The indexed circles correspond to sites, and the cluster decomposition is represented by the dashed lines. Each arrow corresponds to a change in the structure at some precise value of the mutual information cut-off. As a concrete example, we obtain the second decomposition for $0.19 \leq i_{\text{cut}} < 0.25$.

are, and the fraction and properties of resonant pairs. We see a remarkable agreement between the two algorithms, with the sole exception of the fraction of clusters with one hole which is marginally underestimated by less than 0.5% by our main algorithm. The entanglement structure leading to such a difference are two clusters weakly interlaced; taking a set of 6 spins as an example, it would correspond to an optimal bipartition of $\{1, 2, 4\}$ and $\{3, 5, 6\}$ or $\{1, 2, 3, 5\}$ and $\{4, 6\}$. Coupled with the very short range of the pairs and the quasi-absence of sparser structure, the induced change in the properties and distributions is marginal compared to other sources of noise. Indeed, Fig. A4 does not reveal any discrepancy in the distribution.

Appendix B: Cluster decomposition example

We provide in Fig. B1 an example of a decomposition obtained by our algorithm, when we vary the mutual information cut-off introduced in the main text. The state we study was obtained for $L = 10$ and $W = 3.7$.

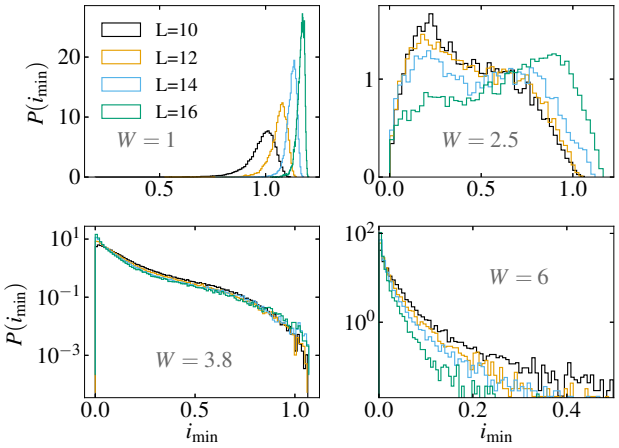

FIG. C1. Probability distribution of the minimal mutual information for different disorder strengths and system sizes. Deep in the ergodic phase, the probability distribution peaks around the (renormalized) thermal entropy. For $W = 2.5$, strong finite-size effects are visible, which correspond to the onset of the transition in small systems. At the phase transition, we observe a decent collapse at intermediate values, though the low-entanglement realizations vastly differ. The average minimal mutual information $\langle i_{\min} \rangle$ decreases with system size as $L^{-0.5\pm0.2}$.

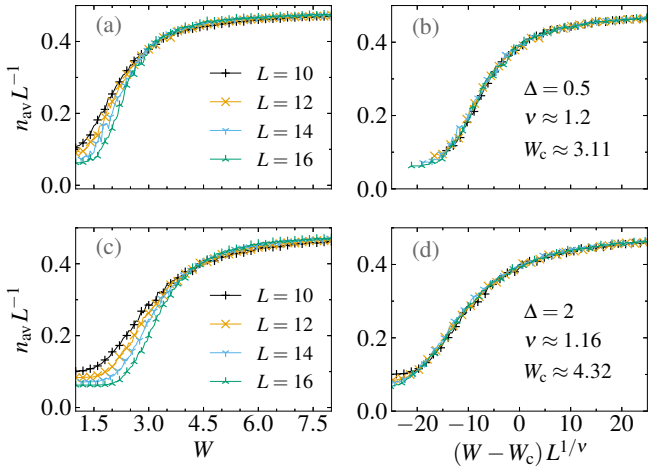

FIG. C2. Statistical average of the mean length of the minimal clusters for two values of the interaction strength Δ, away from the usual Heisenberg limit. (a-b) are taken for $\Delta = 0.5$, while (c-d) correspond to $\Delta = 2$. (b) and (d) are fits to the universal scaling form $n_{\rm av} = L^{-1} f((W - W_c)L^{1/\nu})$. The exponents obtained are similar to the one for $\Delta = 1$.

Appendix C: Complementary numerical results

In this appendix, we provide additional numerical results that support and supplement claims made in the main text.

1. Minimal cluster properties

Figure C1 illustrates the strong finite-size scaling apparent in the minimal mutual information distribution. For $W = 1$, the distribution admits a clear thermal peak, which increases with system size and converges to the thermodynamic thermal value. For $W = 6$, the system has become localized, and the distribution now peaks at $i_{\min} = 0$, with a suppressed tail when system size increases. In between, we observe a cross-over, with an intermediate bimodal distribution at low value of the disorder strength $W = 2.5$. Similar bimodal distributions were observed in other studies on entanglement distributions[8,34,40], but here this bimodality is seemingly only a transient finite-size effect. Close to the estimated phase transition, the distributions collapse decently at intermediate values of $i_{\min}$. Scaling analysis on the characteristic lengths of the minimal clusters also shows a good scaling behavior, as has been shown in the main text.

Figure C2 presents the scaling of the average length of the minimal clusters for different interaction strengths $\Delta = 0.5$ and $\Delta = 2$. In both cases, this quantity acts as an order parameter, with a collapse similar to the one observed for $\Delta = 1$. The critical exponents qualitatively agree with the one observed in the Heisenberg limit.

2. Hierarchical structure at the critical point

Finally, we provide in Fig. C3 explicit examples of the typical entanglement structures observed in states close to or at the critical disorder strength. Strongly entangled small subsets of the system become entangled with other subsets at larger scales. This multiscale structure is strongly indicative of Griffith or fractal states.

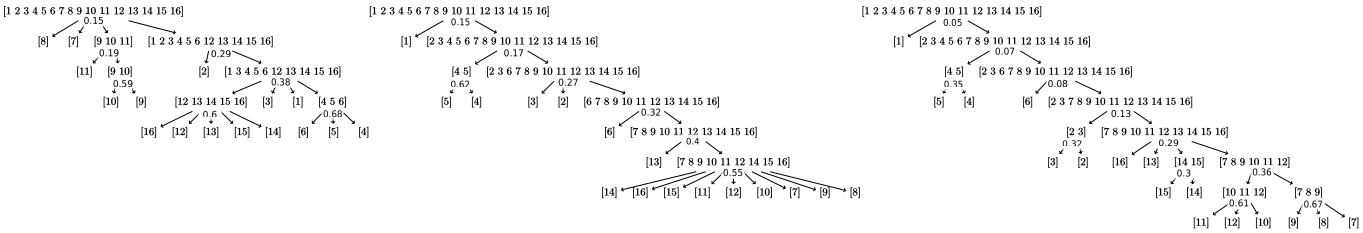

FIG. C3. Three typical examples of the hierarchical multiscale structure obtained for states close to the critical point, with $W = 3.7$ and $L = 16$. Each node corresponds to a cluster, labelled by the sites it includes (here from 1 to 16). The label on the edges corresponds to the mutual information cut-off $i_{\rm cut}$ required to break it into its descendants. For ease of visualization, the data is no longer a binary tree; we have only kept the nodes that appear at the given value of the cut-off, and removed all that are less entangled than their parents (and therefore never appear as a proper cluster). As is readily seen, thermal subclusters (strongly entangled clusters that break into single-site clusters) are present. Clusters can themselves be entangled at larger scales, with a weaker internal entanglement ([1 3 4 5 6 12 13 14 15 16] in the first example, or [7 8 9 10 11 12] in the third one are good examples of such structures).

[1] I. V. Gornyi, A. D. Mirlin, and D. G. Polyakov, "Interacting electrons in disordered wires: Anderson localization and low-t transport," Phys. Rev. Lett. **95**, 206603 (2005).

[2] D. M. Basko, I. L. Aleiner, and B. L. Altshuler, "Metal insulator transition in a weakly interacting many electron system with localized single particle states," Annals of Physics **321**, 1126 – 1205 (2006).

[3] D. A. Abanin and Z. Papi, "Recent progress in many-body localization," Annalen der Physik **529**, 1700169.

[4] F. Alet and N. Laflorencie, "Many-body localization: An introduction and selected topics," Comptes Rendus Physique (2018).

[5] B. Bauer and C. Nayak, "Area laws in a many-body localized state and its implications for topological order," Journal of Statistical Mechanics: Theory and Experiment **2013**, P09005 (2013).

[6] J. A. Kjäll, J. H. Bardarson, and F. Pollmann, "Many-body localization in a disordered quantum ising chain," Phys. Rev. Lett. **113**, 107204 (2014).

[7] D. J. Luitz, "Long tail distributions near the many-body localization transition," Phys. Rev. B **93**, 134201 (2016).

[8] X. Yu, David D. J.. Luitz, and B. K. Clark, "Bimodal entanglement entropy distribution in the many-body localization transition," Phys. Rev. B **94**, 184202 (2016).

[9] M. Serbyn, Z. Papić, and D. A. Abanin, "Local conservation laws and the structure of the many-body localized states," Phys. Rev. Lett. **111**, 127201 (2013).

[10] D. A. Huse, R. Nandkishore, and V. Oganesyan, "Phenomenology of fully many-body-localized systems," Phys. Rev. B **90**, 174202 (2014).

[11] J. Z. Imbrie, "Diagonalization and many-body localization for a disordered quantum spin chain," Phys. Rev. Lett. **117**, 027201 (2016).

[12] J. Z. Imbrie, "On many-body localization for quantum spin chains," Journal of Statistical Physics **163**, 998–1048 (2016).

[13] A. Chandran, C. R. Laumann, and V. Oganesyan, "Finite size scaling bounds on many-body localized phase transitions," arXiv:1509.04285.

[14] V. Ros, M. Müller, and A. Scardicchio, "Integrals of motion in the many-body localized phase," Nuclear Physics B **891**, 420 – 465 (2015).

[15] L. Rademaker and M. Ortuño, "Explicit local integrals of motion for the many-body localized state," Phys. Rev. Lett. **116**, 010404 (2016).

[16] S. Bera, H. Schomerus, F. Heidrich-Meisner, and J. H. Bardarson, "Many-body localization characterized from a one-particle perspective," Phys. Rev. Lett. **115**, 046603 (2015).

[17] S. Bera, T. Martynec, H. Schomerus, F. Heidrich-Meisner, and J. H. Bardarson, "One-particle density matrix characterization of many-body localization," Annalen der Physik **529**, 1600356 (2017).

[18] T. E. O'Brien, D. A. Abanin, G. Vidal, and Z. Papić, "Explicit construction of local conserved operators in disordered many-body systems," Phys. Rev. B **94**, 144208 (2016).

[19] T. L. M. Lezama, S. Bera, H. Schomerus, F. Heidrich-Meisner, and J. H. Bardarson, "One-particle density matrix occupation spectrum of many-body localized states after a global quench," Phys. Rev. B **96**, 060202 (2017).

[20] M. Schreiber, S. S. Hodgman, P. Bordia, H. P. Lüschen, M. H. Fischer, R. Vosk, E. Altman, U. Schneider, and I. Bloch, "Observation of many-body localization of interacting fermions in a quasirandom optical lattice," Science **349**, 842–845 (2015).

[21] J.-Y. Choi, S. Hild, J. Zeiher, P. Schauß, A. Rubio-Abadal, T. Yefsah, V. Khemani, D. A. Huse, I. Bloch, and C. Gross, "Exploring the many-body localization transition in two dimensions," Science **352**, 1547–1552 (2016).

[22] H. P. Lüschen, P. Bordia, S. Scherg, F. Alet, E. Altman, U. Schneider, and I. Bloch, "Observation of slow dynamics near the many-body localization transition in one-dimensional quasiperiodic systems," Phys. Rev. Lett. **119**, 260401 (2017).

[23] M. Žnidarič, T. Prosen, and P. Prelovšek, "Many-body localization in the heisenberg xxz magnet in a random field," Phys. Rev. B **77**, 064426 (2008).

[24] J. H. Bardarson, F. Pollmann, and J. E. Moore, "Unbounded growth of entanglement in models of many-body localization," Phys. Rev. Lett. **109**, 017202 (2012).

[25] M. Serbyn, Z. Papić, and D. A. Abanin, "Universal slow growth of entanglement in interacting strongly disordered systems," Phys. Rev. Lett. **110**, 260601 (2013).

[26] K. Agarwal, E. Altman, E. Demler, S. Gopalakrishnan, D. A. Huse, and M. Knap, "Rare-region effects and dynamics near the many-body localization transition," Annalen der Physik **529**, 1600326 (2017).

[27] D. J. Luitz and Y. B. Lev, "The ergodic side of the many-body localization transition," Annalen der Physik **529**, 1600350 (2017).

[28] S. Roy, Y. B. Lev, and D. J. Luitz, "Anomalous thermalization and transport in disordered interacting floquet systems," Phys. Rev. B **98**, 060201 (2018).

[29] T. L. M. Lezama, S. Bera, and J. H. Bardarson, "Apparent slow dynamics in the ergodic phase of a driven many-body localized system without extensive conserved quantities," arXiv:1809.02894.

[30] A. C. Potter, R. Vasseur, and S. A. Parameswaran, "Universal properties of many-body delocalization transitions," Phys. Rev. X **5**, 031033 (2015).

[31] R. Vosk, D. A. Huse, and E. Altman, "Theory of the many-body localization transition in one-dimensional systems," Phys. Rev. X **5**, 031032 (2015).

[32] L. Zhang, B. Zhao, T. Devakul, and D. A. Huse, "Many-body localization phase transition: A simplified strong-randomness approximate renormalization group," Phys. Rev. B **93**, 224201 (2016).

[33] C. Monthus, "Strong disorder real-space renormalization for the many-body-localized phase of random majorana models," Journal of Physics A: Mathematical and Theoretical **51**, 115304 (2018).

[34] P. T. Dumitrescu, R. Vasseur, and A. C. Potter, "Scaling theory of entanglement at the many-body localization transition," Phys. Rev. Lett. **119**, 110604 (2017).

[35] T. Thiery, F. Huveneers, M. Müller, and W. De Roeck, "Many-body delocalization as a quantum avalanche," Phys. Rev. Lett. **121**, 140601 (2018).

[36] T. Thiery, M. Müller, and W. De Roeck, "A microscopically motivated renormalization scheme for the MBL/ETH transition," arXiv:1711.09880.

[37] A. Goremykina, R. Vasseur, and M. Serbyn, "Analytically solvable renormalization group for the many-body localization transition," arXiv:1807.04285.

[38] F. Iglói and C. Monthus, "Strong Disorder RG approach - a short review of recent developments," arXiv:1806.07684.

[39] P. T. Dumitrescu, S. A. Parameswaran, A. Goremykina, M. Serbyn, and R. Vasseur, In preparation.

[40] V. Khemani, S. P. Lim, D. N. Sheng, and D. A. Huse, "Critical properties of the many-body localization transition," Phys. Rev. X **7**, 021013 (2017).

[41] D. N. Page, "Average entropy of a subsystem," Phys. Rev. Lett. **71**, 1291–1294 (1993).

[42] L. D'Alessio, Y. Kafri, A. Polkovnikov, and M. Rigol, "From quantum chaos and eigenstate thermalization to statistical mechanics and thermodynamics," Advances in Physics **65**, 239–362 (2016).

[43] G. De Tomasi, S. Bera, J. H. Bardarson, and F. Pollmann, "Quantum mutual information as a probe for many-body localization," Phys. Rev. Lett. **118**, 016804 (2017).

[44] J. M. Magn, S. Paganelli, and V. Oganesyan, "Multipoint entanglement in disordered systems," Physics Letters A **381**, 535 – 541 (2017).

[45] M. C. Bañuls, N. Y. Yao, S. Choi, M. D. Lukin, and J. I. Cirac, "Dynamics of quantum information in many-body localized systems," Phys. Rev. B **96**, 174201 (2017).

[46] E. Iyoda and T. Sagawa, "Scrambling of quantum information in quantum many-body systems," Phys. Rev. A **97**, 042330 (2018).

[47] J. A. Kjäll, "Many-body localization and level repulsion," Phys. Rev. B **97**, 035163 (2018).

[48] A. Pal and D. A. Huse, "Many-body localization phase transition," Phys. Rev. B **82**, 174411 (2010).

[49] A. De Luca and A. Scardicchio, "Ergodicity breaking in a model showing many-body localization," EPL (Europhysics Letters) **101**, 37003 (2013).

[50] A. Nanduri, H. Kim, and D. A. Huse, "Entanglement spreading in a many-body localized system," Phys. Rev. B **90**, 064201 (2014).

[51] D. J. Luitz, N. Laflorencie, and F. Alet, "Many-body localization edge in the random-field heisenberg chain," Phys. Rev. B **91**, 081103 (2015).

[52] T. C. Berkelbach and D. R. Reichman, "Conductivity of disordered quantum lattice models at infinite temperature: Many-body localization," Phys. Rev. B **81**, 224429 (2010).

[53] F. Pietracaprina, G. Parisi, A. Mariano, S. Pascazio, and A. Scardicchio, "Entanglement critical length at the many-body localization transition," Journal of Statistical Mechanics: Theory and Experiment **2017**, 113102 (2017).

[54] F. Pietracaprina, N. Macé, D. J. Luitz, and F. Alet, "Shift-invert diagonalization of large many-body localizing spin chains," arXiv:1803.05395.

[55] T. Devakul and R. R. P. Singh, "Early breakdown of area-law entanglement at the many-body delocalization transition," Phys. Rev. Lett. **115**, 187201 (2015).

[56] J. Gray, S. Bose, and A. Bayat, "Many-body localization transition: Schmidt gap, entanglement length, and scaling," Phys. Rev. B **97**, 201105 (2018).

[57] E. V. H. Doggen, F. Schindler, K. S. Tikhonov, A. D. Mirlin, T. Neupert, D. G. Polyakov, and I. V. Gornyi, "Many-body (de)localization in large quantum chains," arXiv:1807.05051.

[58] J. T. Chayes, L. Chayes, D. S. Fisher, and T. Spencer, "Finite-size scaling and correlation lengths for disordered systems," Phys. Rev. Lett. **57**, 2999–3002 (1986).

[59] Z. Lenarčič, E. Altman, and A. Rosch, "Activating many-body localization in solids by driving with light," arXiv:1806.04772.

[60] M. Serbyn and J. E. Moore, "Spectral statistics across the many-body localization transition," Phys. Rev. B **93**, 041424 (2016).

[61] S. D. Geraedts, R. Nandkishore, and N. Regnault, "Many-body localization and thermalization: Insights from the entanglement spectrum," Phys. Rev. B **93**, 174202 (2016).

[62] M. Serbyn, Z. Papić, and D. A. Abanin, "Thouless energy and multifractality across the many-body localization transition," Phys. Rev. B **96**, 104201 (2017).

[63] V. Khemani, F. Pollmann, and S. L. Sondhi, "Obtaining highly excited eigenstates of many-body localized hamiltonians by the density matrix renormalization group approach," Phys. Rev. Lett. **116**, 247204 (2016).

[64] X. Yu, D. Pekker, and B. K. Clark, "Finding matrix product state representations of highly excited eigenstates of many-body localized hamiltonians," Phys. Rev. Lett. **118**, 017201 (2017).

[65] S. P. Lim and D. N. Sheng, "Many-body localization and transition by density matrix renormalization group and exact diagonalization studies," Phys. Rev. B **94**, 045111 (2016).

[66] T. Devakul, V. Khemani, F. Pollmann, D. A. Huse, and S. L. Sondhi, "Obtaining highly excited eigenstates of the localized xx chain via dmrg-x," Philosophical Transactions of the Royal Society of London A: Mathematical, Physical and Engineering Sciences **375** (2017).

[67] M. Serbyn, A. A. Michailidis, D. A. Abanin, and Z. Papić, "Power-law entanglement spectrum in many-body localized phases," Phys. Rev. Lett. **117**, 160601 (2016).

[68] G. Carleo and M. Troyer, "Solving the quantum many-body problem with artificial neural networks," Science **355**, 602–606 (2017).

[69] B. L. Altshuler, Y. Gefen, A. Kamenev, and L. S. Levitov, "Quasiparticle lifetime in a finite system: A nonperturbative approach," Phys. Rev. Lett. **78**, 2803–2806 (1997).

[70] E. J. Torres-Herrera and L. F. Santos, "Extended nonergodic states in disordered many-body quantum systems," Annalen der Physik **529**, 1600284 (2017).

[71] M. Žnidarič, A. Scardicchio, and V. K. Varma, "Diffusive and subdiffusive spin transport in the ergodic phase of a many-body localizable system," Phys. Rev. Lett. **117**, 040601 (2016).

[72] D. J. Luitz, N. Laflorencie, and F. Alet, "Extended slow dynamical regime close to the many-body localization transition," Phys. Rev. B **93**, 060201 (2016).

[73] T. B. Wahl, A. Pal, and S. H. Simon, "Signatures of the Many-body Localized Regime in Two Dimensions," arXiv:1711.02678.

[74] M. Dupont and N. Laflorencie, "Many-body localization as a large family of localized groundstates," arXiv:1807.01313.